International Immunopharmacology 74 (2019) 105663

Contents lists available at ScienceDirect

International Immunopharmacology

journal homepage: www.elsevier.com/locate/intimp

Extracellular vesicles from mesenchymal stem cells prevent contact hypersensitivity through the suppression of Tc1 and Th1 cells and expansion of regulatory T cells

Liyan Guo[a,b,c,1], Peilong Lai[a,b,1], Yulian Wang[a,b], Tian Huang[a,b,c], Xiaomei Chen[a,b], Chenwei Luo[a,b], Suxia Geng[a,b], Xin Huang[a,b], Suijing Wu[a,b], Wei Ling[a,b], Lisi Huang[a,b], Xin Du[a,b,c,*], Jianyu Weng[a,b,c,*]

[a] Department of Hematology, Guangdong Provincial People's Hospital, Guangdong Academy of Medical Sciences, Guangzhou, Guangdong 510080, PR China
[b] Guangdong Provincial Geriatrics Institute, Guangzhou, Guangdong 510080, PR China
[c] South China University of Technology, Guangzhou, Guangdong 510006, PR China

ARTICLE INFO

Keywords:
Extracellular vesicles
Mesenchymal stem cells
Immunoregulation
Contact hypersensitivity
Allergic contact dermatitis

ABSTRACT

Extracellular vesicles (EVs) secreted by mesenchymal stem cells (MSC-EVs) are taken more seriously as immunomodulatory and anti-inflammatory agents. We studied the therapeutic effects of MSC-EVs on allergic contact dermatitis (ACD), a typical T cell-mediated disorder. A contact hypersensitivity (CHS) mouse model for ACD was established and treated by intravenous MSC-EVs injection. We found that human umbilical cord MSC-EVs could significantly prevent the pathology of CHS, including reduced ear swelling and leukocyte infiltration. Injection of MSC-EVs significantly inhibited $CD8^+IFN\text{-}\gamma^+$ cytotoxic T (Tc1) cells and $CD4^+IFN\text{-}\gamma^+$ type 1 helper T (Th1) cells, and reduced the level of pro-inflammatory Tumor Necrosis Factor-alpha (TNF-α) and interferon gamma (IFN-γ), and induced $CD4^+CD25^+Foxp3^+$ regulatory T cells (Tregs) and the level of anti-inflammatory IL-10. *In vitro*, MSC-EVs also suppressed Tc1 and Th1 cells and induced Tregs and the related cytokines, further indicating the immune regulatory role of MSC-EVs. Interestingly, PKH26-labeled MSC-EVs were found to be directly internalized by $CD3^+$ T cells, resulting in reduced signal transducer and activator of transcription 1 (STAT1) protein levels *in vitro*. In summary, MSC-EVs can prevent the onset of CHS by inhibiting Tc1 and Th1 immune responses and inducing the Tregs phenotype *in vivo* and *in vitro*. The mechanism by which MSC-EVs influence $CD3^+$ T cells might partially involve targeting STAT1 *in vitro*. Therefore, MSC-EVs are ideal candidates for cell-free immunomodulatory therapy for T cell-mediated diseases such as ACD.

1. Introduction

Allergic contact dermatitis (ACD), an antigen-specific and type IV delayed hypersensitivity (DTH) reaction in human skin, is a universal occupational health problem [1]. Allergic agents activate antigen-specific T cells, and then induce an inflammatory skin reaction in sensitized patients. Topical corticosteroid application could be applied for palliative ACD, but the outcome is unsatisfactory. Allergen identification can enable contact avoidance, but the process remains challenging. Therefore, more effective desensitizing therapies for ACD patients are urgently needed [2].

As multipotent stromal cells with broad immunomodulatory abilities, mesenchymal stem cells (MSCs) have been utilized to treat various inflammatory and immune-dysregulated diseases in clinical trials [3,4]. MSCs exert a strong regulatory effect on both the innate and adaptive immune responses. MSCs can convert a pro-inflammatory macrophage phenotype to an anti-inflammatory phenotype through the generation of immunosuppressive molecules and metabolites [5,6]. In addition, MSCs can escape T-cell recognition and inhibit excessive T-cell immune responses *e.g.*, they can suppress the activation of Tc1, Th1, and Th17 cells while inducing Tregs differentiation [7]. Although immune therapy using MSCs has achieved great progress, some drawbacks remain including the inconveniences associated with implementing cell-based therapy, high costs, and potential side effects.

* Corresponding authors at: Department of Hematology, Guangdong Provincial People's Hospital, Guangdong Academy of Medical Sciences, Guangzhou 510080, Guangdong, PR China.
E-mail addresses: miyadu@hotmail.com (X. Du), wengjianyu1969@163.com (J. Weng).
[1] These authors contributed equally to the work.

https://doi.org/10.1016/j.intimp.2019.05.048
Received 26 March 2019; Received in revised form 5 May 2019; Accepted 24 May 2019
Available online 12 June 2019
1567-5769/

Notably, MSCs could lead to unwanted long-term side effects because of their potential for uncontrolled differentiation and proliferation. All of these challenges limit the clinical application of MSCs.

Emerging evidence has shown that MSCs exert their immunosuppressive effects by releasing effector agents rather than by cell-cell contact. These cells can naturally produce various sizes of EVs packaged by a lipid bilayer [8]. EVs have two main components: exosomes and microvesicles. Exosomes are the small size EVs with a diameter of 40–150 nm, and formed when the late endosomal compartment sprouts and secreted by fusion with the plasma membrane which encapsulates diverse genetic materials [9]. Microvesicles are the medium/large size EVs range from 100 to 1000 nm, and derived from plasma membrane [10]. EVs are deemed as indispensable mediators of cell communication, which encapsulated diverse genetic materials. MSC-derived EVs (MSC-EVs) have the potential to convey regulatory molecules that can modulate immune cell function [11,12]. Of note, MSC-EVs have been shown to possess similar immunomodulatory abilities as that observed for MSCs. Therefore, we speculated that MSC-EVs may be a novel therapeutic for desensitizing against allergic diseases.

Therefore, we investigated the immunomodulatory functions of MSC-EVs in a CHS mice model for human ACD. CHS mice experience two distinct phases during the pathological process: a sensitization phase and an elicitation phase. When allergens contact the skin, they activate innate immunity and release numerous pro-inflammatory cytokines. These cytokines are recognized by Langerhans cells and dermal dendritic cells. These cells can transport antigens to skin-draining lymph nodes where the activation and differentiation of allergen-specific T lymphocytes occurs [13]. After re-exposure, allergen-specific T lymphocytes are re-activated to produce the inflammatory cytokines and chemokines that lead to destructive cutaneous inflammation [14]. Thus, we studied the therapeutic effects of MSC-EVs on ACD in CHS mice and clarified the underlying mechanisms.

2. Materials and methods

2.1. Characterization of human umbilical cord MSCs (hucMSCs)

Human umbilical cord samples were obtained after cesarean delivery with the mother's written informed consent at the Guangdong Provincial People's Hospital of China and processed within 6 h. There were fifteen human umbilical card samples, with age range from twenty-six to forty and an average age at 32.5 ± 1.2, were used for the isolation of MSC-EVs. The healthy donors were included without abnormal immune indicators, such as hepatitis antibodies, antithyroid antibodies and so on. Umbilical cord samples were gently cut into small pieces after removing the umbilical cord tunica and arteriovenous vessels, and the jelly was digested with collagenase II (Invitrogen, Carlsbad, CA, USA) to obtain cells [15]. The adherent cells were planted in hucMSC complete medium (Cyagen, Suzhou, China) at 37 °C with 5% CO_2. The hucMSCs began to proliferate significantly after one week. At 80% integration, the cells were isolated and passaged. Only the third generation of hucMSCs was used in our study.

Prior to experimental use, the multi-differentiation abilities of hucMSCs were identified by inducing differentiation into osteoblasts, adipocytes, and chondrocytes. Briefly, passage 3 cells were cultured in complete media to induce the differentiation of osteoblasts, adipocytes, or chondrocytes. After three weeks of culture, the hucMSCs were washed, fixed, and stained with Alizarin Red for 5 min or Oil-Red-O for 30 min. After four weeks of culture for chondrogenic pellet formation, pellets were fixed, embedded, sectioned, and then stained with Safranin O. All of the chemical reagents mentioned above were purchased from Cyagen, China. In addition, the surface marker expression profiles of the hucMSCs were obtained to confirm the expression of surface biomarker. hucMSCs were labeled with fluorophore-conjugated specific antibodies anti-CD73 (REF12073942), anti-CD31 (REF12031942), anti-CD34 (REF12034942), anti-CD45 (REF17045942), anti-CD105 (REF17105742), anti-CD166 (REF12166842), anti-CD29 (REF17029942), anti-CD44 (REF11044182), anti-CD90 (REF11090942), anti-CD14 (REF17014942), anti-CD19 (REF11019942), and anti-HLA-DR (REF11995242) for 25 min (all from eBioscience, San Diego, CA, USA). According to the recommendations of the International Society of Cell Therapy, the expression profiles needed to meet the minimum standard for defining human MSCs [16].

Table 1
Primers used for real-time PCR.

Gene primer sequence (5′-3′)		
Mus-TNF-α	F	CAGACCCTCACACTCACAAACCAC
Mus-TNF-α	R	CCTTGTCCCTTGAAGAGAACCTG
Mus-IFN-γ	F	AGTTCTGGGCTTCTCCTCCT
Mus-IFN-γ	R	GGCTTTCAATGACTGTGCCG
Mus-IL-10	F	GGAAGACAATAACTGCACCCACT
Mus-IL-10	R	CAACCCAAGTAACCCTTAAAGTCC
Mus-GAPDH	F	AAGAAGGTGGTGAAGCAGG
Mus-GAPDH	R	GAAGGTGGAAGAGTGGGAGT

2.2. Isolation of MSC-EVs

MSCs (5×10^5 cells) were cultured in 10 cm dishes at passage 3. At 80% confluence, MSCs were washed three times after the supernatants were discarded, and then serum-free medium (Stem Pro® MSC SFM CTS™; Gibco, Grand Island, NY, USA) was added. We then collected the supernatants after 2 d. HucMSC-EVs (human umbilical cord MSCs derived EVs) were harvested as previously described [17]. Briefly, culture supernatants were centrifuged at 300 ×*g* for 10 min followed by 2000 ×*g* for 20 min to remove cells and debris, and they were then centrifuged at 10,000 ×*g* to remove large proteins. The supernatants were then passed through a 0.22 μm filter membrane to separate large EVs. The supernatants were next ultra-centrifuged at 100,000 ×*g* for 90 min using a horizontal rotor (SW32 Ti, Beckman Coulter, Miami, FL, USA) to isolate small/medium EVs. The pelleted EVs were resuspended and ultra-centrifuged again at 100,000 ×*g* for 90 min, and the final EVs pellets were stored at −80 °C.

2.3. Characterization of MSC-EVs

The morphology of MSC-EVs was analyzed by transmission electron microscopy (TEM; Hitachi, Tokyo, Japan) [17]. Briefly, MSC-EVs suspensions were dropped onto a copper grid, stained with aqueous phosphotungstic acid, and then observed by TEM. The size distribution of the MSC-EVs was analyzed by Nanoparticle Tracking Analysis (NTA; NanoSight NS500, Malveron Instruments, Orsay) using the following parameters: camera level 11, threshold 2, and three videos per sample. The protein concentrations of the MSC-EVs were detected by the Bradford protein assay (Thermo Fisher Scientific, Waltham, MA, USA). For immunoblot analysis, 10 μg of MSC-EVs and supernatants were lysed, separated, transferred, and then incubated with antibodies directed against human CD9 (sc-13118, Santa Cruz Biotechnology, Santa Cruz, CA, USA), CD63 (sc-5275, Santa Cruz Biotechnology, Santa Cruz, CA, USA) and TSG101 (sc-7964, Santa Cruz Biotechnology, Santa Cruz, CA, USA) to detect purified MSC-EVs.

2.4. Animals

Six-week-old male BALB/c mice were from the Animal Center of Beijing Vital River Laboratory Animal Technology Company in China. All of the animal experiments were conducted with the guidance of the Sun Yat-sen University Cancer Center and approved by the Ethical Committee and Institutional Animal Care and Use Committee of the Center. And the number of Ethical Committee Agreement for our

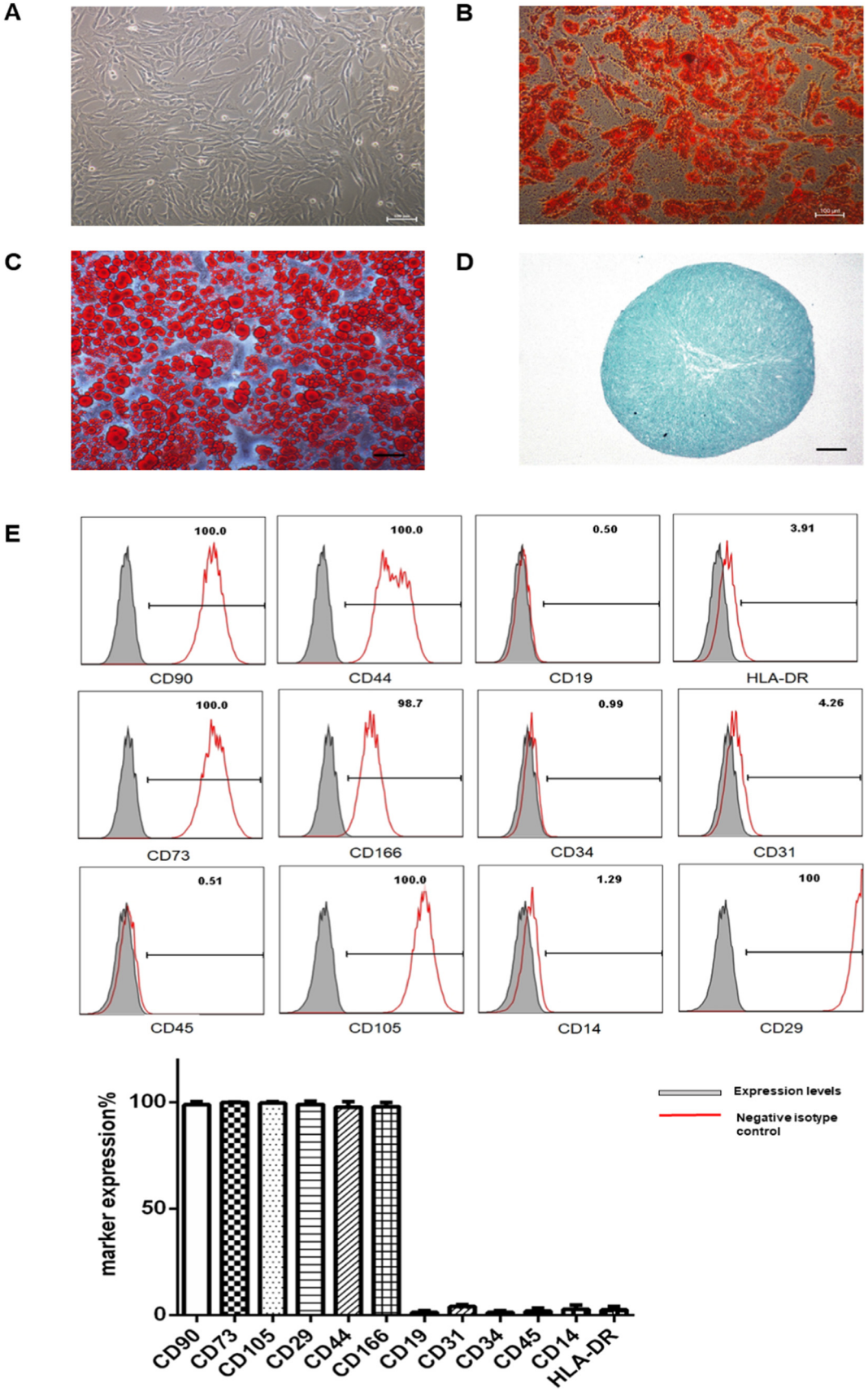

(caption on next page)

Fig. 1. Characteristics of hucMSCs and MSC-EVs.
A. Representative image of the fibroblast-like and adherent morphology of hucMSCs at passage three. Scale bar, 100 μm. The multi-lineage differentiation ability of hucMSCs. B. Alizarin Red staining of osteocytes that developed after culturing hucMSCs in osteogenic medium for 3 weeks. C. Oil Red O staining of adipocytes that developed after culturing hucMSCs in adipogenic medium for 3 weeks. Scale bar, 100 μm. D. Alcian Blue staining of chondrocytes that developed after culturing hucMSCs in chondrogenic medium for 4 weeks. Scale bar, 100 μm. E. Flow cytometry analysis of hucMSCs surface markers. Data = mean ± SD (n = 3). The filled gray curves indicate unstained controls.

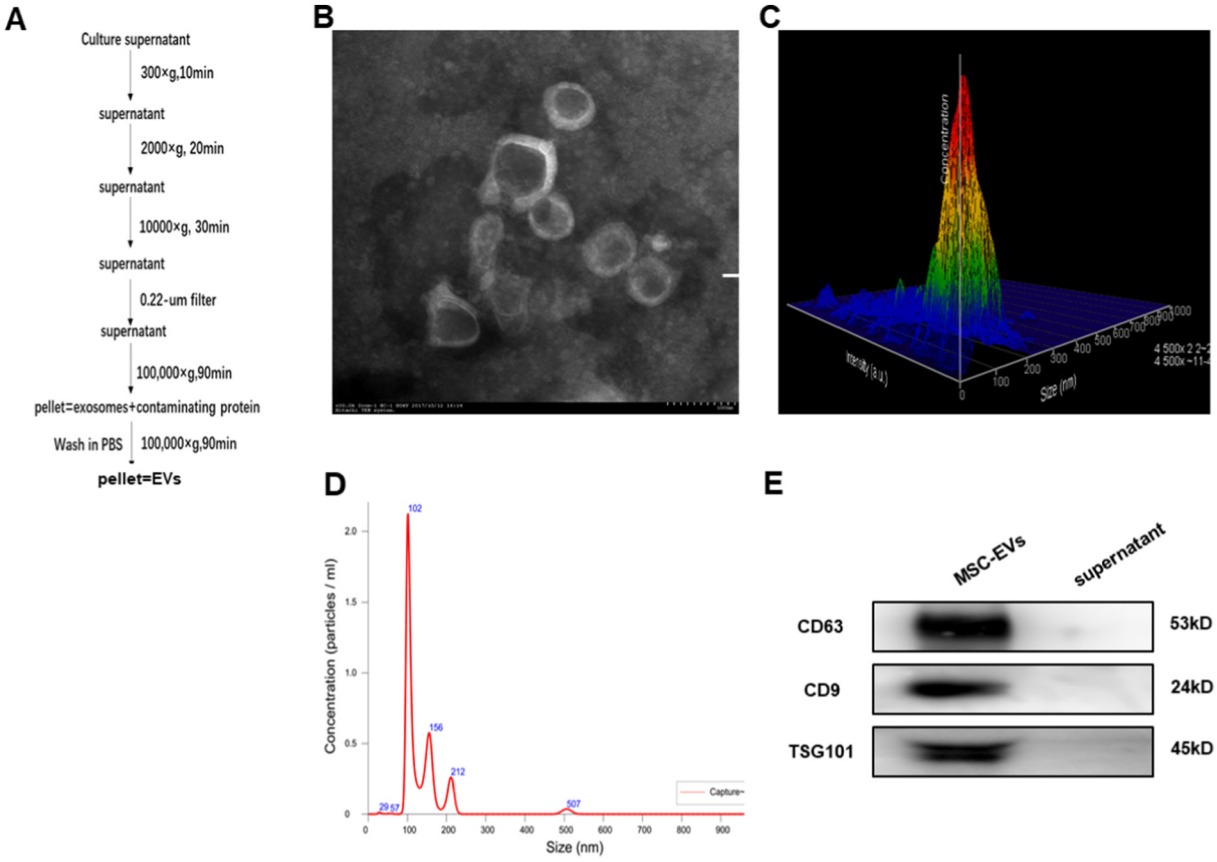

Fig. 2. Characterization of MSC-EVs.
A. Experimental protocol for isolating EVs by differential ultracentrifugation. B. Transmission electron microscopy image of the saucer-like morphology of MSC-EVs. Scale bar, 100 nm. C–D. NTA demonstrating the size distribution of the MSC-EVs. Camera level 11, threshold 2, and three videos per sample. The particles ranged from 96.4 nm (D10) to 201.5 nm (D90) with most of the particles ~101.2 nm. E. Equal amounts of protein from the MSC-EVs preparation and culture supernatant were analyzed for the EVs-enriched proteins CD9, CD63 and TSG101 by Western blot. The MSC-EVs, but not the supernatant, were positive for CD9, CD63 and TSG101.

animals study is L102012018040C.

2.5. Mouse model for CHS and ear swelling measurements

The establishment of a CHS model was similar to a method previously described [18,19]. Briefly, mice of the same weight were selected, and a 2 cm^2 area was shaved on the back of each mouse as the first contact sensitized area (sensitization). A total of 25 μl of 0.5% 2,4-dinitro-1-fluorobenzene (DNFB, D1529; Sigma-Aldrich, St. Louis, MO, USA), which was dissolved in acetone/olive oil at a 4:1 mixture, was evenly spread on the back. After five days, the right ear of each CHS mouse was treated with 20 μl of 0.2% DNFB as the second contact initiation area (elicitation). The animals were separated into three groups: control (PBS, n = 8, sensitization only), CHS (CHS mice with PBS, n = 8), and MSC-EVs (CHS mice with MSC-EVs, n = 8). To assess the therapeutic effects of MSC-EVs on CHS mice, the same volume of PBS or 100 μg MSC-EVs were intravenously injected on day 1 post-elicitation. We used micrometer calipers (Mitutoyo, Kawasaki, Kanagawa, Japan) to measure the degree of ear swelling daily and calculate ear swelling by the thickness of the ear that underwent elicitation minus that of the ear that did not. The units of ear swelling response are micron (μm). Four days after elicitation, we isolated ear samples, peripheral blood, and cervical lymph nodes (LNs).

2.6. Hematoxylin-eosin (HE) staining

Left ear tissues were collected and fixed in 10% formaldehyde, dehydrated *via* a series of ethanol washes, permeated with xylene, and paraffin-embedded. After dewaxing and hydration, samples were stained with HE and observed by light microscopy.

2.7. Isolation of human peripheral blood mononuclear cells (PBMCs)

PBMCs were isolated from fresh whole blood from 10 young healthy volunteers (ages 20–40 years old, 5 females and 5 males) who signed informed consent. The Ethical Committee of the Guangdong Provincial People's Hospital approved this protocol. PBMCs were prepared from peripheral blood diluted in phosphate buffer saline (PBS), slowly added to Lymphoprep, and then centrifuged. The separated PBMCs were collected and washed twice with PBS using centrifugation. $CD3^+$ T cells

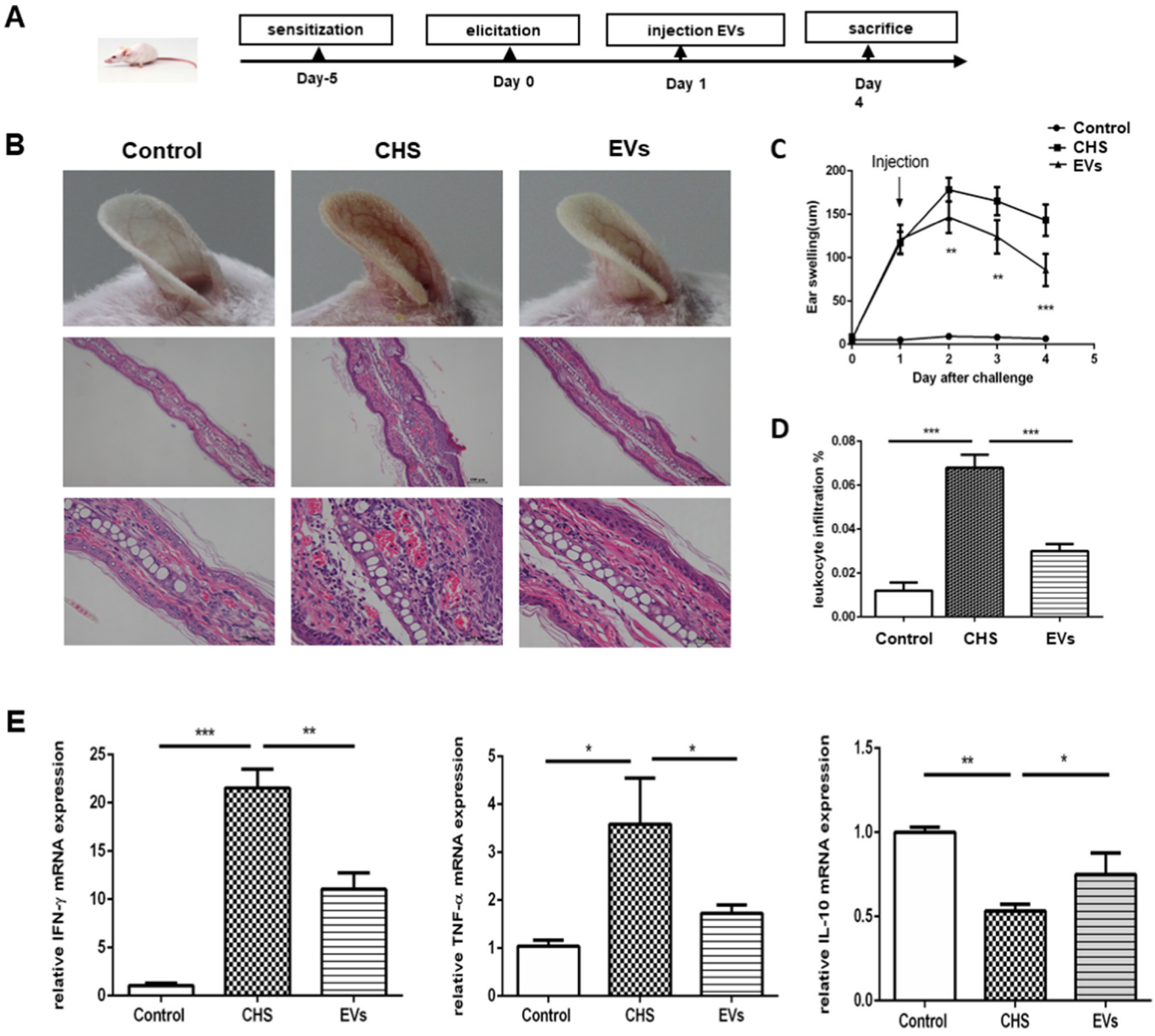

Fig. 3. MSC-EVs prevent the manifestations of CHS ears.
A. Experimental protocol for the CHS model. DNFB hapten was used for sensitization. There were three groups in this experiment: control (no elicitation, no CHS manifestation; PBS, n = 8), CHS (CHS + PBS, n = 8), and MSC-EVs (CHS + MSC-EVs, n = 8). Experimental mice were intravenously injected with PBS or MSC-EVs on day 1 after elicitation. B. Ear swelling, hardness, inflammatory liquid and histopathological damage were showed in the picture. Representative photos and HE-stained samples of ears from each group. The scales or magnification were uniform in the three groups. Scale bars, 100 μm (up) and 50 μm (down). C. The ear swelling was continuously recorded for 4 d after elicitation in different group. The units of ear swelling response are micron (μm). We used micrometer calipers to measure the degree of ear swelling daily and calculated ear swelling as the thickness of elicitation ears minus the thickness of the control ears. Data = mean ± SD (n = 6). **, $p < 0.01$, ***, $p < 0.001$. D. Percentage of leukocyte infiltration in HE-stained ear samples. Data = mean ± SD (n = 6). **, $p < 0.01$, ***, $p < 0.001$. E. The relative level of IFN-γ, TNF-α, and IL-10 mRNA expression in CHS ears. Data = mean ± SD (n = 3). *, $p < 0.05$, **, $p < 0.01$.

were then isolated from PBMCs using anti-human CD3 MicroBeads (Miltenyi Biotec, Bergisch Gladbach, Germany).

2.8. Co-culture of PBMCs with MSC-EVs

PBMCs (5×10^5 cells/ml) were plated in RPMI 1640 complete medium and stimulated by adding 2.5 μg/ml phytohemagglutinin (PHA; Sigma-Aldrich, St. Louis, MO, USA). PHA-stimulated PBMCs (PHA-PBMCs) were co-cultured with the same volume of PBS or MSC-EVs (10 or 50 μg/ml) for 4 d. The percentage of $CD8^+IFN\text{-}\gamma^+$ Tc1, $CD4^+IFN\text{-}\gamma^+$ Th1, and $CD4^+CD25^+Foxp3^+$ Tregs and the concentration of cytokines were measured.

2.9. Flow cytometry analysis

For analysis of LNs and peripheral blood of mice and human PBMCs, cells were incubated with fluorophore-conjugated specific antibodies directed against CD3, CD8, CD25, and CD4 or respective isotype controls at room temperature for 25 min. For intracellular staining, we first stimulated cells with cell stimulation cock tail plus protein transport inhibitors (REF004975, eBioscience, San Diego, CA, USA) for 5 h. These cells were surface-stained with antibodies against CD3, CD4, or CD8 or their respective isotype controls for 25 min and then fixed and permeabilized with Perm/Fix solution (eBioscience, San Diego, CA, USA; or MultiSciences, Hangzhou, China). Finally, antibodies against IFN-γ

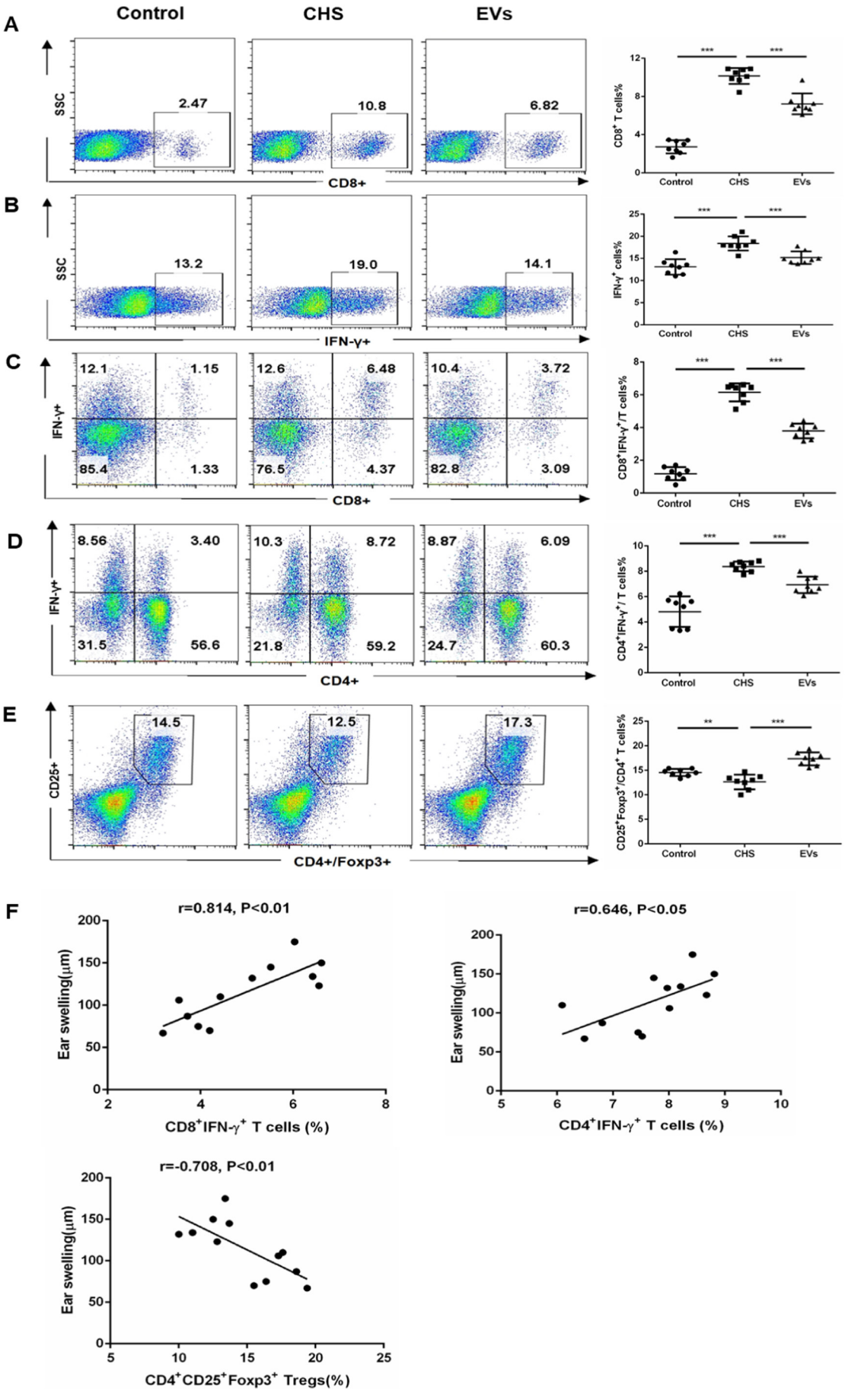

(caption on next page)

Fig. 4. MSC-EVs inhibited $CD8^+IFN\text{-}\gamma^+$ Tc1 and $CD4^+IFN\text{-}\gamma^+$ Th1 cells, induced $CD4^+CD25^+Foxp3^+$ Tregs in the cervical LNs of mice.
A–E. Frequencies of $CD8^+$ T cells, $IFN\text{-}\gamma^+$ cells, $CD8^+IFN\text{-}\gamma^+$ Tc1 cells, $CD4^+IFN\gamma^+$ Th1 cells, and $CD4^+CD25^+Foxp3^+$ Tregs cells were analyzed by flow cytometry. The first cervical LNs were collected 4 d after elicitation. In panel E, we gated the $CD25^+Foxp3^+$ cells in $CD4^+$ gate. Data = mean ± SD. n = 8 mice/group. **, $p < 0.01$, ***, $p < 0.001$. F. The correlation analysis between the percentage of $CD8^+IFN\text{-}\gamma^+$ Tc1 cells or $CD4^+TNF\text{-}\alpha^+$ Th1 cells or $CD4^+CD25^+Foxp3^+$ Tregs and the ear swelling (elicitation ears minus the thickness of the control ears; μm) of CHS mice treatment with PBS or MSC-EVs 4 d after elicitation. Data = mean ± SD. n = 6 mice/group. Pearson correlation analysis was used. *, $p < 0.05$, **, $p < 0.01$. Pearson $r > 0$ represents the positive correlation. Pearson $r < 0$ represents the negative correlation.

or Foxp3 or isotype control were added for 25 min. All antibodies were obtained from eBioscience, San Diego, CA, USA (anti-human CD3, REF11003842; anti-human CD4, REF11004842; anti-human CD8, REF25008742; anti-human CD25, REF12025980; anti-human IFN-γ, REF17731982; anti-human Foxp3, REF17477642; anti-Mouse CD4, REF11004182; anti-Mouse CD8, REF25008182; anti-Mouse IFN-γ, REF17731182; anti-Mouse CD25, REF12025182; anti-Mouse Foxp3, REF17577382). To avoid endocytosis of the CD4 antigen epitope, we used $CD3^+CD8^-$ T cells to select for $CD4^+$ T cells co-cultured *in vitro* with PHA-PBMCs and MSC-EVs [20,21]. With the same method mentioned above, we only observed endocytosis of the CD4 antigen in human PBMCs but not in the LNs and the peripheral blood of mice. Phorbol myristate acetate (PMA) can induce endocytosis of CD4, and PMA was included in cell stimulation cock. Study showed that PMA-induced down-modulation of CD4 among various cell types, and the effects were greater for human PBL [20]. All flow cytometry data were acquired using the FACS Canto II cytometer (Becton Dickinson, San Jose, CA, USA) and analyzed with Flowjo 10 software (Tree Star, London, Britain).

2.10. Cytokine measurements

Serum samples were collected from CHS mice 4 d after elicitation. Supernatants from *in vitro* co-cultures were harvested after 4 d and stored at −80 °C. A Luminex MAGPIX system (Luminex Corp, Austin, TX) was used to detect the concentrations of TNF-α, IFN-γ, and IL-10 in mouse serum, and an enzyme-linked immunosorbent assay (ELISA; R&D Systems, Minneapolis, MN, USA) was used to detect supernatants IL-10, TNF-α, and IFN-γ levels.

2.11. RNA isolation, reverse transcription, and real-time quantitative PCR (qRT-PCR)

Ear samples were isolated 4 d after elicitation and total RNA was extracted from ear tissues using Trizol reagent, according to the manufacturer's protocol (Invitrogen, Carlsbad, CA, USA). RNA concentration and purity were determined by measuring absorbances at 260 nm and 280 nm. The OD260/OD280 purity between 1.8 and 2.0 could be used for downstream processing. Reverse transcription was performed to synthetic cDNA according to the manufacturer's instructions (TaKaRa, Tokyo, Japan). Subsequently, qRT-PCR was performed using the SYBR Green PCR Master Mix (TaKaRa, Tokyo, Japan) with Applied Biosystems 7500 (Applied Biosystems, Foster City, CA, USA). GAPDH was used as an internal control for normalization. The $2^{-\Delta\Delta Ct}$ method was used to calculate the relative gene expression. All experiments were conducted at least in triplicate. The sequences of the primers are shown in Table 1.

2.12. MSC-EVs labeling

Isolated MSC-EVs were stained with the PKH26 labeling kit (Sigma-Aldrich, St. Louis, MO, USA). Briefly, 10 μg MSC-EVs were mixed with PKH26 red fluorescent dye in 1 ml of diluent C solution and incubated for 5 min. A negative control lacking EVs was used to detect carryover from the PKH26 dye. After labeling, the MSC-EVs were washed with an equal volume of complete culture media, which removed EVs by ultracentrifugation to stop the labeling reaction. Then, the appropriate amount of PBS was added followed by ultra-centrifugation at 100,000 × *g* for 90 min. PKH26-labeled MSC-EVs were resuspended with PBS after discarding the supernatant. To explore whether MSC-EVs could directly interact with $CD3^+$ T cells, we added PKH26-labeled MSC-EVs (10 μg) to $CD3^+$ T cells and cultured them for 12 h, which was then centrifuged, fixed with formaldehyde and blocked with bovine serum albumin followed by labeling of the cytoskeleton with Alexa Fluor Phalloidin-488 (Invitrogen, Carlsbad, CA, USA) for 30 min. Nuclei were counterstained with DAPI (Invitrogen, Carlsbad, CA, USA). A confocal microscope (Zeiss LSM800, Germany) equipped with ZEN lite software was used to analyze images.

2.13. Western blots

After PHA-$CD3^+$ T cells (2.5 μg/ml) were cultured with PBS or MSC-EVs (50 μg/ml) for 4 d, the cells were simultaneously lysed and separated in 10% Tris-Glycine SDS PAGE gels, and western blots analysis was performed using primary antibodies directed against human STAT1 (Rabbit mAb, 14994T, Cell Signaling Technology (CST), Danvers, MA, USA), pSTAT1 (Rabbit mAb, #7649, CST, Danvers, MA, USA), and GAPDH (Rabbit mAb, ab181602, Abcam, Cambridge, MA, USA). The secondary antibody used was anti-rabbit IgG (7074S, CST, Danvers, MA, USA). The Pre-stained Protein Ladder was used in our experiments (26616, Thermo Fisher Scientific, Waltham, MA, USA). ImageJ was used for grayscale analysis.

2.14. Statistical analysis

The data are presented as the mean ± standard deviation for the results from at least three independent experiments. Statistical Product and Service Solutions (SPSS) software version 13.0 (IBM, Ehningen, Germany) and GraphPad Prism 6.0 software (La Jolla, CA, USA) were employed to analyze the data. The *t*-test and one-way analysis of variance (ANOVA) tests were used to analyze the statistical significance of differences between two groups or among multiple groups, respectively. Pearson correlation analysis was used to detect the correlation between two variables. Pearson correlation coefficient (r) > 0 represents the positive correlation, and $r < 0$ represents the negative correlation. A *p*-value < 0.05 was regarded statistically significant.

3. Results

3.1. Characteristics of hucMSCs

HucMSCs are adherent cells with a long-spindle morphology, and the picture in Fig. 1A shows a representative image for passage 3. Under different differentiation conditions, hucMSCs can be induced to form osteoblasts (Fig. 1B), adipocytes (Fig. 1C), or chondrocytes (Fig. 1D) as identified by staining with different reagents, confirming the multilineage differentiation ability of hucMSCs. In addition, the expression of MSC surface markers was confirmed by flow cytometry. The results demonstrated that hucMSCs were positive for CD73, CD105, CD166, CD29, CD44, and CD90, which are mesenchymal or cell adhesion markers, but negative for CD14, CD19, CD31, CD34, CD45, and HLA-DR (Fig. 1E). Thus, the cultured cells met the minimum standards defined for MSCs [16].

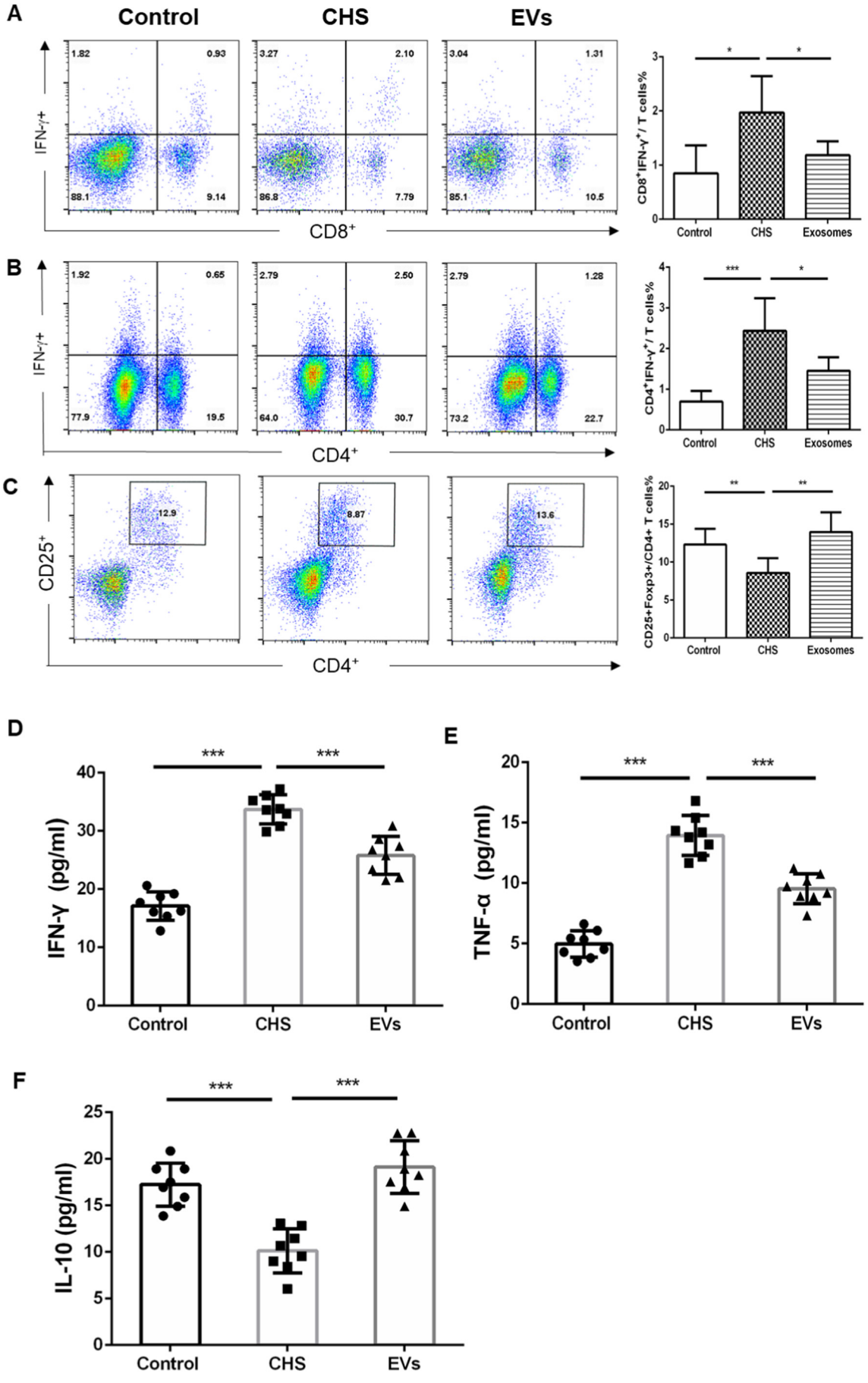

(caption on next page)

Fig. 5. MSC-EVs inhibit Tc1 and Th1, and induce Tregs, and change the related cytokine in the peripheral blood of CHS mice.
A–C. The changes of T cells in the peripheral blood of CHS mice after elicitation for 4 d. $CD8^+IFN\text{-}\gamma^+$ Tc1 cells and $CD4^+IFN\text{-}\gamma^+$ Th1 cells was reduced, and $CD4^+CD25^+Foxp3^+$ Tregs ($CD25^+Foxp3^+$ in $CD4^+$ gate in panel C) was increased after MSC-EVs therapy compared with the CHS group with PBS. The concentration of the cytokines TNF-α, IFN-γ, and IL-10 in plasma obtained 4 d post-elicitation. Data = mean ± SD. n = 6 mice/group. **$p < 0.01$, ***$p < 0.001$. D–F. IFN-γ and TNF-α were observably higher in the CHS group than the control group, and they were decreased in CHS mice upon treatment with MSC-EVs. The IL-10 levels were significantly lower in the CHS group compared with the control group, and there was an increased in CHS mice upon treatment with MSC-EVs. Data = mean ± SD. n = 8 mice/group. **$p < 0.01$, ***$p < 0.001$.

3.2. Characterization of MSC-EVs

MSC-EVs were isolated using the gold standard ultracentrifugation method (Fig. 2A). Generally, 400 ml supernatant of one donative hucMSCs at passage three (almost 4×10^7–6×10^7 cells) produced approximately 305.2 ± 72.3 μg of small/medium MSC-EVs. TEM demonstrated that MSC-EVs had a saucer-like morphology (Fig. 2B). NTA demonstrated that the size distribution of the particles in the MSC-EVs preparation ranged from 96.4 nm (D10) to 201.5 nm (D90) with most particles measured approximately 101.2 nm (Fig. 2C–D). These particles were almost the small and medium EVs. In our study, 100 μg EVs had almost $(1.58 \pm 0.47) \times 10^{10}$ pellets measured by nanoparticle tracking analysis. Finally, western blotting demonstrated that MSC-EVs, but not the supernatant, were positive for CD9, CD63 and TSG101, which are transmembrane proteins or cytosolic proteins enriched in EVs (Fig. 2E). These data indicated that the particles isolated from MSCs were small/medium EVs.

3.3. MSC-EVs prevent the pathological changes of CHS ears

To evaluate whether MSC-EVs could attenuate ACD symptoms *in vivo*, we established a CHS mice model by contacting the same antigen twice, intravenously injecting with PBS or MSC-EVs on day 1 post-elicitation, and then measuring external ear swelling and thickness every 24 h (Fig. 3A). We found that treatment with MSC-EVs markedly reduced ear thickness (μm) after injection after 1 d ($p < 0.01$), 2 d ($p < 0.01$), and 3 d ($p < 0.001$) (Fig. 3C). As expected, histopathological damage, including ear swelling, hardness, inflammatory liquid, and leukocyte infiltration were prominent in the PBS-treated mice (control *versus* CHS, $p < 0.001$), whereas treatment with MSC-EVs prevented damage from occurring (MSC-EVs *versus* PBS, $p < 0.001$, Fig. 3B and D). We also explored TNF-α, IFN-γ and IL-10 mRNA expression levels in CHS ear tissues. Results showed that the relative expression of pro-inflammatory cytokines IFN-γ and TNF-α were significantly increased, and this trend were relieved after the CHS mice were treated with MSC-EVs. The level of IL-10 mRNA was reduced in the CHS mice while MSC-EVs treatment increased IL-10 (Fig. 3E). Our experimental results demonstrate that MSC-EVs efficiently prevent the onset of CHS responses *in vivo*.

3.4. MSC-EVs inhibit $CD8^+IFN\text{-}\gamma^+$ Tc1, $CD4^+IFN\text{-}\gamma^+$ Th1 cells, and induce $CD4^+CD25^+Foxp3^+$ Tregs in cervical lymph nodes of mice

ACD pathogenesis in the CHS model requires IFN-γ polarity driven by $CD8^+$ and $CD4^+$ T helper cells with receptors for DNFB. It has been shown that induction of CHS lead to the increasing of Tc1 and Th1 effector cells and the reduction of Tregs [22–24]. In this study, we isolated the cervical draining LNs where effector T cells were activated by antigen presenting cells (APCs) to induce DTH, and studied the T-cell immune responses in the draining LNs after treatment with MSC-EVs. As expected, the percentages of the $CD8^+$ T cells ($p < 0.001$), $IFN\text{-}\gamma^+$ cells ($p < 0.001$), $CD8^+IFN\text{-}\gamma^+$ Tc1 cells ($p < 0.001$), and $CD4^+IFN\text{-}\gamma^+$ Th1 cells ($p < 0.001$) increased in the cervical LNs of CHS mice. In contrast, $CD8^+$ T cells ($p < 0.001$), $IFN\text{-}\gamma^+$ cells ($p < 0.001$), $CD8^+IFN\text{-}\gamma^+$ Tc1 cells ($p < 0.001$), and $CD4^+IFN\text{-}\gamma^+$ Th1 cells ($p < 0.001$) were reduced in cervical LNs isolated from CHS mice treated with MSC-EVs (Fig. 4A–D). In addition, there were fewer $CD4^+CD25^+Foxp3^+$ Tregs in the CHS mice compared with the control group ($p < 0.01$). Furthermore, treatment with MSC-EVs dramatically increased Tregs ($p < 0.001$) (Fig. 4E). Then the correlation analysis between the percentage of $CD8^+IFN\text{-}\gamma^+$ Tc1 cells or $CD4^+IFN\text{-}\gamma^+$ Th1 cells or $CD4^+CD25^+Foxp3^+$ Tregs and the ear swelling of CHS mice treatment with PBS or MSC-EVs were measured 4 d after elicitation. As expected, the percentage of Tc1 cells and Th1 cells were positively related to the ear swelling ($r = 0.814$, $p < 0.01$ and $r = 0.646$, $p < 0.05$ respectively). And the percentage of Tregs was significantly negatively related to the ear swelling ($r = -0.708$, $p < 0.01$) (Fig. 4F). These results demonstrate that MSC-EVs prevented the progression of CHS *via* inhibiting Tc1 and Th1 immunoreaction and inducing Tregs.

3.5. MSC-EVs inhibit Tc1 and Th1, and induce Tregs, and change the related cytokine in the peripheral blood of CHS mice

To explore that whether the changes of those cells appeared in the peripheral blood of CHS mice since MSC-EVs were intravenously injected in mice. We studied the changes of T cells in the peripheral blood of CHS mice after elicitation for 4 d. And we found that MSC-EVs therapy can significantly reduce the percentages of $CD8^+IFN\text{-}\gamma^+$ Tc1 cells ($p < 0.001$) and $CD4^+IFN\text{-}\gamma^+$ Th1 cells ($p < 0.001$), and increase $CD4^+CD25^+Foxp3^+$ Tregs ($p < 0.01$) compared with the CHS group with PBS (Fig. 5A–C). The trend of those cells was the same as that in the LNs of mice. The activation and proliferation of T lymphocytes release inflammatory cytokines IFN-γ, TNF-α, and anti-inflammatory cytokine IL-10 and play important roles in CHS pathophysiology; thus, we investigated whether MSC-EVs could influence the release of CHS-related cytokines. We found that the concentrations of IFN-γ ($p < 0.001$) and TNF-α ($p < 0.001$) were increased, and IL-10 ($p < 0.001$) was decreased in the plasma of CHS mice compared with the control group. However, upon MSC-EVs treatment, this trend was reversed where IFN-γ ($p < 0.001$) and TNF-α ($p < 0.001$) were decreased, and IL-10 was increased ($p < 0.001$) (Fig. 5D–F).

3.6. MSC-EVs exhibit similar immunosuppressive effects when co-cultured with human PBMCs in vitro

We also examined the immunosuppressive effects of MSC-EVs *in vitro* by treating human PHA-PBMCs with different doses of MSC-EVs (10 or 50 μg/ml) for 4 d. Treatment with 10 or 50 μg/ml MSC-EVs significantly reduced $CD8^+IFN\text{-}\gamma^+$ Tc1 ($p < 0.01$ and $p < 0.001$) and $CD4^+IFN\text{-}\gamma^+$ Th1 cells ($p < 0.01$ and $p < 0.001$) (Fig. 6A–B) and increased $CD4^+CD25^+Foxp3^+$ Tregs ($p < 0.001$ and $p < 0.001$) (Fig. 6C), but the alterations were more prominent in the 50 μg/ml group. ELISA was used to detect the concentrations of IFN-γ, TNF-α and IL-10 in culture media containing PHA-PBMCs with PBS or MSC-EVs (10 and 50 μg/ml). The results demonstrated a significant dose-dependent reduction in the concentrations of IFN-γ and TNF-α in the MSC-EVs group compared with the control group (Fig. 6D–E). The level of IL-10, which plays a crucial part in suppressing immune responses, increased in a dose-dependent manner in response to treatment with MSC-EVs ($p < 0.001$) (Fig. 6F). These data indicate that MSC-EVs exhibit immunomodulatory effect *via* inducing Tregs and anti-inflammatory cytokines IL-10, and suppressing Th1 and Tc1 cells progression and the release of pro-inflammatory cytokines *in vitro*.

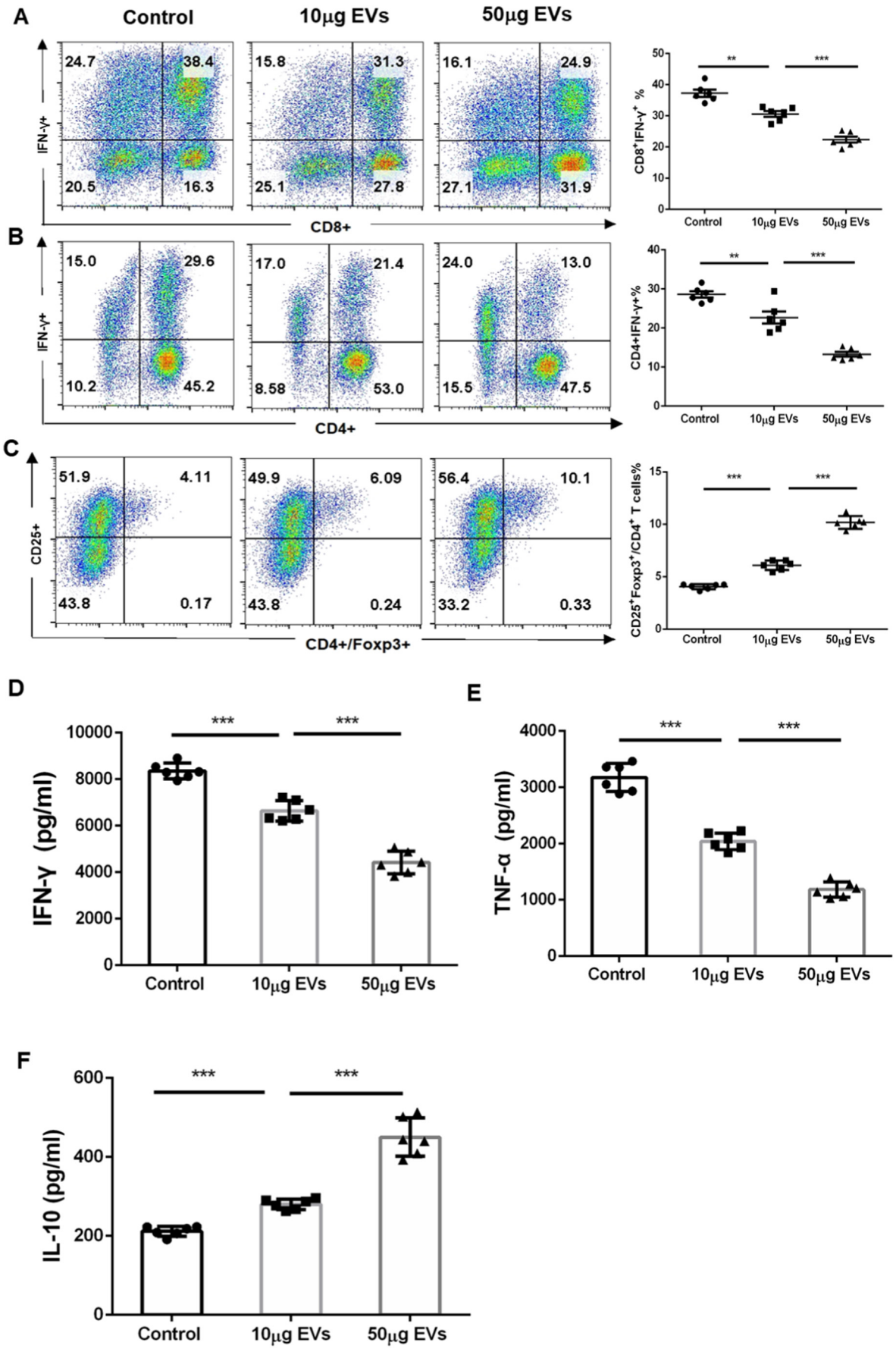

(caption on next page)

Fig. 6. MSC-EVs exhibit similar immunosuppressive effects when co-cultured with human PBMCs *in vitro*.
A–C. The percentage of $CD8^+IFN\text{-}\gamma^+$ Tc1 cells, $CD4^+IFN\text{-}\gamma^+$ Th1 cells and $CD4^+CD25^+Foxp3^+$ Tregs were detected after PHA-PBMCs incubated with PBS or MSC-EVs (10 μg or 50 μg/ml) for 4 d *in vitro*. In panel B, we gated $CD3^+CD8^-$ cells to represent $CD4^+$ T cells. And in panel C, we gated the $CD25^+Foxp3^+$ cells in $CD4^+$ gate. Data = mean ± SD (n = 6). **, $p < 0.01$, ***, $p < 0.001$. D–F. The levels of IFN-γ, TNF-α and IL-10 in conditioned media from PHA-PBMCs treatment with 10 or 50 μg/ml MSC-EVs for 4 d *in vitro* were measured by ELISA. MSC-EVs significantly decreased IFN-γ and TNF-α in a dose-dependent manner, and increased IL-10 in a dose-dependent manner. Data = mean ± SD (n = 6). ***, $p < 0.001$.

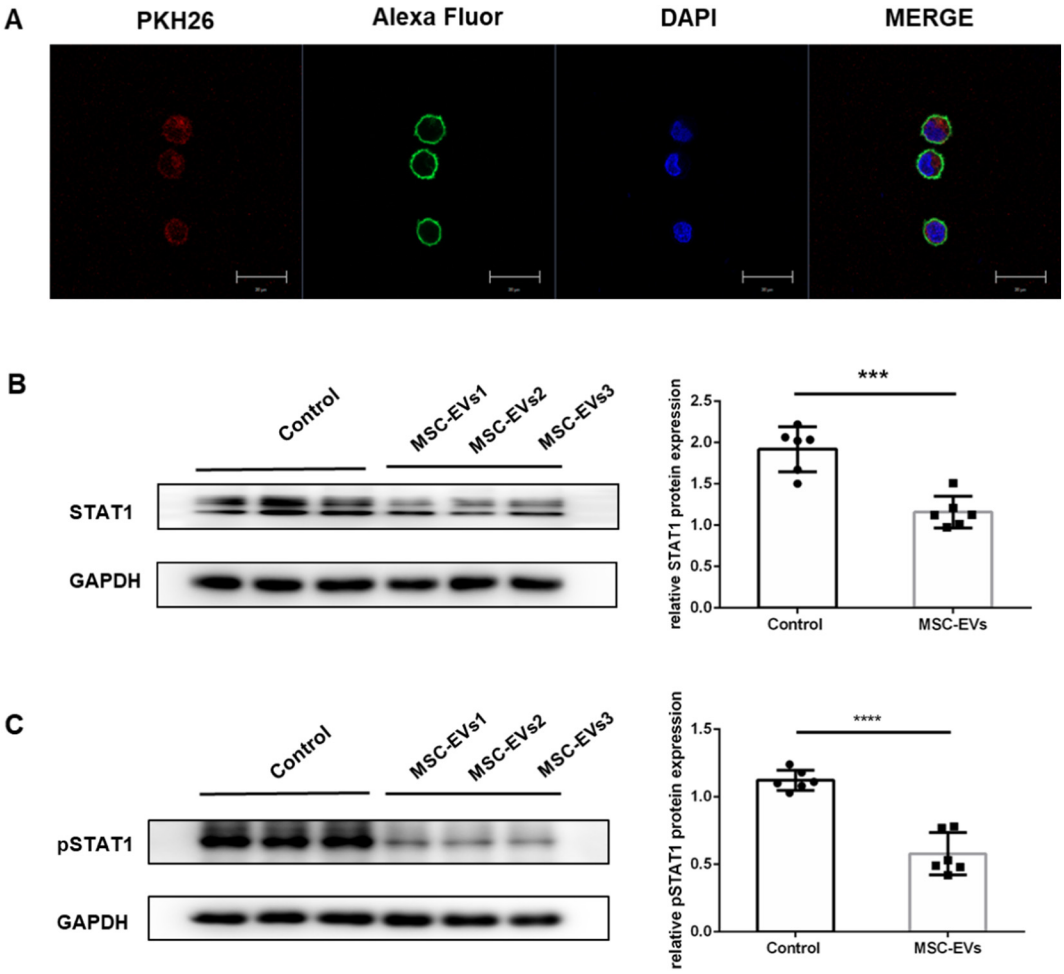

Fig. 7. Direct interaction between MSC-EVs and $CD3^+$ T cells *in vitro*.
A. The association between MSC-EVs and PHA-stimulated $CD3^+$ T cells was observed by confocal microscopy. Isolated $CD3^+$ T cells were cultured with PKH26-labeled MSC-EVs (red) for 12 h and then immunolabeled with Alexa Fluor Phalloidin-488 conjugated to FITC (green). Nuclei from $CD3^+$ T cells were stained with DAPI (blue). The image shows that PKH26-labeled MSC-EVs are associated with the nuclei of $CD3^+$ T cells. Scale bar, 20 μm. B–C. The relative protein levels of STAT1 and pSTAT1 after co-culturing $CD3^+$ T cells with 50 μg MSC-EVs for 4 d. Treatment with MSC-EVs significantly reduces the protein expression of STAT1 and pSTAT1. Data = mean ± SD (n = 6). ***, $p < 0.001$. (For interpretation of the references to color in this figure legend, the reader is referred to the web version of this article.)

3.7. MSC-EVs influence $CD3^+$ T cells might partially involve targeting STAT1 in vitro

To determine whether MSC-EVs are internalized and have any effect on $CD3^+$ T cells, cells were pre-incubated with PKH26-stained MSC-EVs for 12 h and analyzed by immunofluorescence. We found that MSC-EVs and $CD3^+$ T cells consistently co-localize, indicating that MSC-EVs exert their function by directly interacting with $CD3^+$ T lymphocytes (Fig. 7A). After co-culturing $CD3^+$ T cells with different MSC donor-derived EVs for 4 d, we observed that treatment with MSC-EVs dramatically lowered the expression level of STAT1 and pSTAT1, indicating that MSC-EVs induce Tregs and inhibit Tc1 and Th1 cells may partially by suppressing STAT1 activation *in vitro* (Fig. 7B–C). Therefore, MSC-EVs may exert their immunomodulatory function on $CD3^+$ T cells possibly by targeting STAT1 and pSTAT1 *in vitro*.

4. Discussion

The pathogenesis of CHS results from the dynamics and complexity of cell immune and molecular inflammatory networks. During CHS, hapten-specific T cells secrete IFN-γ, TNF-α, and other inflammatory mediators that elicit immune responses and amplify inflammatory reactions when the same hapten is encountered again [25,26]. In contrast, Tregs have been demonstrated to prevent the development of allergic reactions to haptens that contact the skin and restrict the magnitude of the inflammatory response in sensitized individuals [2,27,28]. We show for the first time that MSC-EVs exert their immunomodulatory effects through multiple inflammatory signaling pathways using a mouse CHS model. MSC-EVs suppressed the development of Th1 and Tc1 cells, and decreased the expression of IFN-γ and TNF-α *in vivo* and *in vitro*. In addition, MSC-EVs promoted the

expansion of Tregs and expression of IL-10, an anti-inflammatory cytokine that prevents antigen presentation and immune cell activation.

Many studies have shown that MSC-EVs possess the same therapeutic abilities as their parental MSCs to prevent the onset of inflammation. In experimental autoimmune encephalomyelitis, a study showed that mouse bone marrow MSC-derived EVs (BM-MSC-EVs), which included the MSC-derived tolerogenic molecules PD-L1, galectin-1, and TGF-β1, inhibited autoreactive lymphocyte propagation and induced the generation of anti-inflammatory cytokines. This report also showed that MSC-EVs induced tolerogenic signaling by stimulating the production of Tregs and inducing the apoptosis of activated T lymphocytes [29]. In autoimmune murine models of experimental autoimmune uveoretinitis, MSC-EVs effectively prevent the onset of the diseases, inhibit the activation and proliferation of APCs, Th1 and Th17 cells [30]. In addition, MSC-EVs alleviated manifestations of severe steroid refractory GVHD in recipients of hematopoietic stem cell transplantation. In this study, the patient presented with reduced IL-1β, TNF-α, and IFN-γ levels, and an increased IL-10 after treatment with MSC-EVs [31]. Consistent with previous observations, we found that MSC-EVs exerted therapeutic effects in the CHS mouse model.

MicroRNAs (miRNAs) can be a major functional component of EVs that is transferred to receptor cells to regulate the communication of genetic information [32,33]. When STAT1 signaling is activated, STAT1 migrates to the nucleus to bind the IFN-γ activation sequence and drive the expression of target genes. These genes induce a cellular antiviral state, thus influencing the proliferation of T cells, such as Tc1, Th1, and Tregs [34,35]. Our molecular mechanism studies demonstrated that MSC-EVs could be directly internalized by $CD3^+$ T cells and thus influence them by reducing the level of STAT1 protein and its phosphorylation *in vitro*. In our study, STAT1 signaling inhibition also indicates that it is a crucial pathway for MSC-EVs-mediated regulation of $CD3^+$ T cells. Various miRNAs can regulate STAT1 to affect downstream mechanisms. For example, miR-181 and miR-150 attenuate dendritic cell (DC) immunoreaction by targeting JAK/STAT1 signaling [36]. MiR-146a plays a central role within the STAT1/IFN-γ axis in the melanoma microenvironment [37]. Furthermore, MSC-EVs are rich in bound miRNAs that regulate the STAT1 gene, such as miR-146a, miR-181, and miR-21 [38–40]. In future studies, we will identify the key miRNA and/or protein molecules in MSC-EVs that modulate immune responses and alleviate autoimmune disorder symptoms.

Before administration of EVs can be extensively implemented in clinics, some issues must be resolved. First, effective and safe EVs doses and treatment times need to be standardized to treat specific diseases, and delivery routes, such as intranasal administration or direct dispersive injection into wounds, must be optimized [41]. Additionally, methods to stimulate the release of EVs, such as increasing cytosolic Ca^{2+} levels [10], to mass-produce EVs and reduce the cost of production without compromising the contents and functions of EVs remain to be elucidated. To fully translate the beneficial effects of MSC-EVs treatment into the clinic, cell culture conditions for EVs collection must be optimized. Finally, specific genetic modifications in EVs might enhance immunogenicity and therapeutic efficacy.

In conclusion, our study demonstrates that MSC-EVs ameliorate CHS and exert immunomodulatory effects on $CD8^+$ cytotoxic Tc1 cells and $CD4^+$ Th1 cells. MSC-EVs also suppressed the production of the inflammatory mediators, including IFN-γ and TNF-α. Importantly, MSC-EVs upregulated the percentage of immune-tolerant cells, including Tregs, and cytokines such as IL-10, to sensitizing haptens. The underlying mechanism may be partially due to the targeting of STAT1 and pSTAT1 on T cells. These findings suggest that MSC-EVs administration could be a beneficial, cell-free treatment for ACD and autoimmune diseases.

Declaration of Competing Interest

The authors declare that there are no competing financial interests in relation to the work described here.

Acknowledgments

This work was supported by the National Natural Science Foundation of China (grant number 81870121, 81671585, 81500102, and 81370665); the Science and Technology Planning Project of Guangdong Province, China (grant number 2014B020212009, 2014B020226002, 2015B020227003, 2015B020226001, and 2017B020230004); the Science and Technology Planning Project of Guangzhou, China (grant number 201803040005, 201803040011, and 201400000003-4); and the Project of Administration of Traditional Chinese Medicine of Guangdong Province of China (grant number. 20191008).

References

[1] N. Dhingra, A. Shemer, J. Correa da Rosa, M. Rozenblit, J. Fuentes-Duculan, J.K. Gittler, R. Finney, T. Czarnowicki, X. Zheng, H. Xu, Y.D. Estrada, I. Cardinale, M. Suarez-Farinas, J.G. Krueger, E. Guttman-Yassky, Molecular profiling of contact dermatitis skin identifies allergen-dependent differences in immune response, J. Allergy Clin. Immunol. 134 (2014) 362–372.

[2] W.R. Su, Q.Z. Zhang, S.H. Shi, A.L. Nguyen, A.D. Le, Human gingiva-derived mesenchymal stromal cells attenuate contact hypersensitivity via prostaglandin E2-dependent mechanisms, Stem Cells 29 (2011) 1849–1860.

[3] S. Wang, X. Qu, R.C. Zhao, Clinical applications of mesenchymal stem cells, J. Hematol. Oncol. 5 (2012) 19.

[4] M.J. Hoogduijn, F. Popp, R. Verbeek, M. Masoodi, A. Nicolaou, C. Baan, M.H. Dahlke, The immunomodulatory properties of mesenchymal stem cells and their use for immunotherapy, Int. Immunopharmacol. 10 (2010) 1496–1500.

[5] Y. Kawata, A. Tsuchiya, S. Seino, Y. Watanabe, Y. Kojima, S. Ikarashi, K. Tominaga, J. Yokoyama, S. Yamagiwa, S. Terai, Early injection of human adipose tissue-derived mesenchymal stem cell after inflammation ameliorates dextran sulfate sodium-induced colitis in mice through the induction of M2 macrophages and regulatory T cells, Cell Tissue Res. 376 (2) (2019) 257–271.

[6] W.J. Song, Q. Li, M.O. Ryu, J.O. Ahn, D. Ha Bhang, Y. Chan Jung, H.Y. Youn, TSG-6 secreted by human adipose tissue-derived mesenchymal stem cells ameliorates DSS-induced colitis by inducing M2 macrophage polarization in mice, Sci. Rep. 7 (2017) 5187.

[7] P. Luz-Crawford, M. Kurte, J. Bravo-Alegria, R. Contreras, E. Nova-Lamperti, G. Tejedor, D. Noel, C. Jorgensen, F. Figueroa, F. Djouad, F. Carrion, Mesenchymal stem cells generate a CD4+CD25+Foxp3+ regulatory T cell population during the differentiation process of Th1 and Th17 cells, Stem Cell Res Ther 4 (2013) 65.

[8] C. Thery, K.W. Witwer, Minimal Information for Studies of Extracellular Vesicles 2018 (MISEV2018): A Position Statement of the International Society for Extracellular Vesicles and Update of the MISEV2014 Guidelines, 7 (2018), p. 1535750.

[9] B. Fevrier, G. Raposo, Exosomes: endosomal-derived vesicles shipping extracellular messages, Curr. Opin. Cell Biol. 16 (2004) 415–421.

[10] J. Ratajczak, M. Wysoczynski, F. Hayek, A. Janowska-Wieczorek, M.Z. Ratajczak, Membrane-derived microvesicles: important and underappreciated mediators of cell-to-cell communication, Leukemia 20 (2006) 1487–1495.

[11] B. Zhang, Y. Yin, R.C. Lai, S.S. Tan, A.B. Choo, S.K. Lim, Mesenchymal stem cells secrete immunologically active exosomes, Stem Cells Dev. 23 (2014) 1233–1244.

[12] P. Lai, X. Chen, L. Guo, Y. Wang, X. Liu, Y. Liu, T. Zhou, T. Huang, S. Geng, C. Luo, X. Huang, S. Wu, W. Ling, X. Du, C. He, J. Weng, A potent immunomodulatory role of exosomes derived from mesenchymal stromal cells in preventing cGVHD, J. Hematol. Oncol. 11 (2018) 135.

[13] S.F. Martin, T. Jakob, From innate to adaptive immune responses in contact hypersensitivity, Curr. Opin. Allergy Clin. Immunol. 8 (2008) 289–293.

[14] J.K. Gittler, J.G. Krueger, E. Guttman-Yassky, Atopic dermatitis results in intrinsic barrier and immune abnormalities: implications for contact dermatitis, J. Allergy Clin. Immunol. 131 (2013) 300–313.

[15] Y.F. Han, R. Tao, T.J. Sun, J.K. Chai, G. Xu, J. Liu, Optimization of human umbilical cord mesenchymal stem cell isolation and culture methods, Cytotechnology 65 (2013) 819–827.

[16] M. Dominici, K. Le Blanc, I. Mueller, I. Slaper-Cortenbach, F. Marini, D. Krause, R. Deans, A. Keating, D. Prockop, E. Horwitz, Minimal criteria for defining multipotent mesenchymal stromal cells. The International Society for Cellular Therapy position statement, Cytotherapy 8 (2006) 315–317.

[17] C. Thery, S. Amigorena, G. Raposo, A. Clayton, Isolation and characterization of exosomes from cell culture supernatants and biological fluids, Curr. Protoc. Cell Biol. 30 (1) (2006) 3.22.1–3.22.29 (Chapter 3: Unit 3.22).

[18] J.L. Garrigue, J.F. Nicolas, R. Fraginals, C. Benezra, H. Bour, D. Schmitt, Optimization of the mouse ear swelling test for in vivo and in vitro studies of weak contact sensitizers, Contact Dermatitis 30 (1994) 231–237.

[19] X. Zhang, W. Huang, X. Chen, Y. Lian, J. Wang, C. Cai, L. Huang, T. Wang, J. Ren, A.P. Xiang, CXCR5-overexpressing mesenchymal stromal cells exhibit enhanced homing and can decrease contact hypersensitivity, Mol. Ther. 25 (2017) 1434–1447.

[20] M. Bigby, P. Wang, J.F. Fierro, M.S. Sy, Phorbol myristate acetate-induced down-modulation of CD4 is dependent on calmodulin and intracellular calcium, J. Immunol. 144 (1990) 3111–3116.
[21] C.H. Zhang, G. Grunig, W. Davis, D.F. Antczak, Down-regulation followed by re-expression of equine CD4 molecules in response to phorbol myristate acetate, Vet. Immunol. Immunopathol. 42 (1994) 71–82.
[22] M.J. Glass, P.R. Bergstresser, R.E. Tigelaar, J.W. Streilein, UVB radiation and DNFB skin painting induce suppressor cells universally in mice, J. Invest. Dermatol. 94 (1990) 273–278.
[23] A. Maeda, S. Beissert, T. Schwarz, A. Schwarz, Phenotypic and functional characterization of ultraviolet radiation-induced regulatory T cells, J. Immunol. 180 (2008) 3065–3071.
[24] B. Wang, H. Fujisawa, L. Zhuang, I. Freed, B.G. Howell, S. Shahid, G.M. Shivji, T.W. Mak, D.N. Sauder, CD4+ Th1 and CD8+ type 1 cytotoxic T cells both play a crucial role in the full development of contact hypersensitivity, J. Immunol. 165 (2000) 6783–6790.
[25] M. Vocanson, A. Hennino, M. Cluzel-Tailhardat, P. Saint-Mezard, J. Benetiere, C. Chavagnac, F. Berard, D. Kaiserlian, J.F. Nicolas, CD8+ T cells are effector cells of contact dermatitis to common skin allergens in mice, J. Invest. Dermatol. 126 (2006) 815–820.
[26] S. Nakae, H. Suto, M. Kakurai, J.D. Sedgwick, M. Tsai, S.J. Galli, Mast cells enhance T cell activation: importance of mast cell-derived TNF, Proc. Natl. Acad. Sci. U. S. A. 102 (2005) 6467–6472.
[27] S. Ring, S.J. Oliver, B.N. Cronstein, A.H. Enk, K. Mahnke, CD4+CD25+ regulatory T cells suppress contact hypersensitivity reactions through a CD39, adenosine-dependent mechanism, J. Allergy Clin. Immunol. 123 (e1282) (2009) 1287–1296.
[28] S. Ring, S. Karakhanova, T. Johnson, A.H. Enk, K. Mahnke, Gap junctions between regulatory T cells and dendritic cells prevent sensitization of CD8(+) T cells, J. Allergy Clin. Immunol. 125 (2010) (237-246.e231-237).
[29] A. Mokarizadeh, N. Delirezh, A. Morshedi, G. Mosayebi, A.A. Farshid, K. Mardani, Microvesicles derived from mesenchymal stem cells: potent organelles for induction of tolerogenic signaling, Immunol. Lett. 147 (2012) 47–54.
[30] T. Shigemoto-Kuroda, J.Y. Oh, D.K. Kim, H.J. Jeong, S.Y. Park, H.J. Lee, J.W. Park, T.W. Kim, S.Y. An, D.J. Prockop, R.H. Lee, MSC-derived extracellular vesicles attenuate immune responses in two autoimmune murine models: type 1 diabetes and uveoretinitis, Stem Cell Rep. 8 (2017) 1214–1225.
[31] L. Kordelas, V. Rebmann, A.K. Ludwig, S. Radtke, J. Ruesing, T.R. Doeppner, M. Epple, P.A. Horn, D.W. Beelen, B. Giebel, MSC-derived exosomes: a novel tool to treat therapy-refractory graft-versus-host disease, Leukemia 28 (2014) 970–973.
[32] L. Zhang, S. Zhang, J. Yao, F.J. Lowery, Q. Zhang, W.C. Huang, P. Li, M. Li, X. Wang, C. Zhang, H. Wang, K. Ellis, M. Cheerathodi, J.H. McCarty, D. Palmieri, J. Saunus, S. Lakhani, S. Huang, A.A. Sahin, K.D. Aldape, P.S. Steeg, D. Yu, Microenvironment-induced PTEN loss by exosomal microRNA primes brain metastasis outgrowth, Nature 527 (2015) 100–104.
[33] W. Ying, M. Riopel, G. Bandyopadhyay, Y. Dong, A. Birmingham, J.B. Seo, J.M. Ofrecio, J. Wollam, A. Hernandez-Carretero, W. Fu, P. Li, J.M. Olefsky, Adipose tissue macrophage-derived exosomal miRNAs can modulate in vivo and in vitro insulin sensitivity, Cell 171 (2017) 372–384 (e312).
[34] J. Wen, Y. Zhou, J. Wang, J. Chen, W. Yan, J. Wu, J. Yan, K. Zhou, Y. Xiao, Y. Wang, Q. Xia, W. Cai, Interactions between Th1 cells and Tregs affect regulation of hepatic fibrosis in biliary atresia through the IFN-gamma/STAT1 pathway, Cell Death Differ. 24 (2017) 997–1006.
[35] X. Liu, W. Mo, J. Ye, L. Li, Y. Zhang, E.C. Hsueh, D.F. Hoft, G. Peng, Regulatory T Cells Trigger Effector T Cell DNA Damage and Senescence Caused by Metabolic Competition, 9 (2018), p. 249.
[36] J. Zhu, K. Yao, J. Guo, H. Shi, L. Ma, Q. Wang, H. Liu, W. Gao, A. Sun, Y. Zou, J. Ge, miR-181a and miR-150 regulate dendritic cell immune inflammatory responses and cardiomyocyte apoptosis via targeting JAK1-STAT1/c-Fos pathway, J. Cell. Mol. Med. 21 (2017) 2884–2895.
[37] J. Mastroianni, N. Stickel, miR-146a Controls Immune Response in the Melanoma Microenvironment, 79 (2019), pp. 183–195.
[38] Q. Cheng, X. Li, J. Liu, Q. Ye, Y. Chen, Multiple Myeloma-derived Exosomes Regulate the Functions of Mesenchymal Stem Cells Partially Via Modulating miR-21 and miR-146a, 2017 (2017), p. 9012152.
[39] Y. Fu, L. Zhang, F. Zhang, T. Tang, Q. Zhou, C. Feng, Y. Jin, Z. Wu, Exosome-mediated miR-146a Transfer Suppresses Type I Interferon Response and Facilitates EV71 Infection, 13 (2017), p. e1006611.
[40] G. Kohanbash, H. Okada, MicroRNAs and STAT interplay, Semin. Cancer Biol. 22 (2012) 70–75.
[41] Q. Long, D. Upadhya, B. Hattiangady, D.K. Kim, S.Y. An, B. Shuai, D.J. Prockop, A.K. Shetty, Intranasal MSC-derived A1-exosomes ease inflammation, and prevent abnormal neurogenesis and memory dysfunction after status epilepticus, Proc. Natl. Acad. Sci. U. S. A. 114 (2017) E3536–e3545.